

Emergence of collective propulsion through cell-cell adhesion

Katsuyoshi Matsushita

Department of Biological Sciences, Osaka University, Toyonaka, Osaka, Japan

The mechanisms driving the collective movement of cells remain poorly understood. To contribute toward resolving this mystery, a model was formulated to theoretically explore the possible functions of polarized cell-cell adhesion in collective cell migration. The model consists of an amoeba cell with polarized cell-cell adhesion, which is controlled by positive feedback with cell motion. This model cell has no persistent propulsion, and therefore exhibits a simple random walk when in isolation. However, at high density, these cells acquire collective propulsion and form ordered movement. This result suggests that cell-cell adhesion has a potential function, which induces collective propulsion with persistence.

Collective cell migration is an indispensable element for various developmental, physiological, and pathological processes [1–3]. However, the guiding mechanisms driving the movement of cells during migration are not sufficiently understood. Various biological hypotheses have been proposed to elucidate these mechanisms [4], which have been examined in the field of physics [5–15]. One of the most widely investigated hypotheses is based on the concept of a leader cell that differentiates to lead other cells [16]. Another major hypothesis is extracellular matrix (ECM) leading, including durotaxis [17] and haptotaxis [18]. Along with these models, various other hypothetical guiding mechanisms can qualitatively reproduce many aspects of collective cell migration.

Among these mechanisms, the most simple guiding principle is one in which homogeneous cells mutually lead themselves independently of the ECM, which is referred to here as the “mutual leading mechanism.” In spite of the simplicity of this type of guiding, it induces rich collective behavior [19]. In these behaviors, leading is based on cell-cell communication. Chemotaxis is a major communication tool used for cellular interactions [20] as observed in the aggregation of *Dictyostelium discoideum* [21] and in contact inhibition of the locomotion of neural crest cells [15, 22]. Therefore, investigations of the mutual leading mechanism conducted to date have mainly focused on the chemotactic response of cells [23].

Another possible communication tool is cell-cell adhesion [24]. In contrast to the in-depth understanding of the functions of chemotaxis in collective cell migration, knowledge of the role of cell-cell adhesion is limited. In particular, although the role of cell-cell adhesion in the leader cell mechanism has been recently clarified [16, 25, 26], its role in the mutual leading mechanism remains largely unclear. Cell-cell adhesion can possibly act as a driving force for collective behavior [27], including the alignments of *Dictyostelium discoideum* [28, 29] and the neural crest [30]. To intuitively consider the functions of cell-cell adhesion in these types of cells, I begin with a thought experiment using a model amoeba cell population that exhibits cell-cell adhesion, as shown in Fig. 1(a). When a cell leads other cells to align their directions of movement via cell-cell adhesion, single-side polarization in cell-cell adhesion is necessary. This is be-

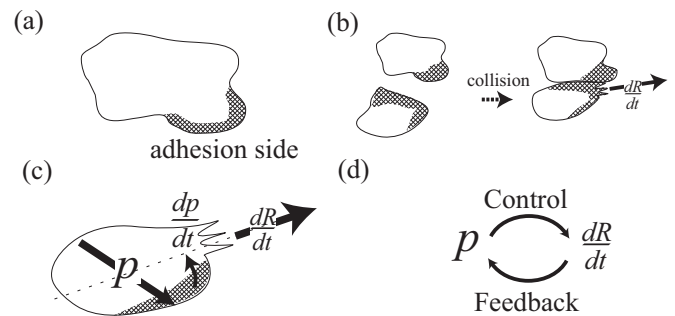


FIG. 1. (a) Schematic view of a model cell with polarized cell-cell adhesion. The shaded region represents a high-strength region of cell-cell adhesion. (b) The collision process of two cells. The arrows represent cell movement. $d\mathbf{R}/dt$ represents the direction of cell motion. The saw tooth shape of the bottom cell represents the protrusion that induces cell movement. The two cells collide and are then bound through cell-cell adhesion. As a result, the cells move in essentially the same direction. (c) Dynamics of polarized cell-cell adhesion. The arrow of \mathbf{p} represents the direction of single-side polarized cell-cell adhesion and the curved arrow represents $d\mathbf{p}/dt$ according to Eq. 1. The dotted line indicates the direction of $d\mathbf{R}/dt$. (d) Schematic relation between \mathbf{p} and $d\mathbf{R}/dt$.

cause cells cannot indicate a certain direction of movement through isotropic cell-cell adhesion. This type of polarized cell-cell adhesion promotes the protrusion of other cells toward the direction of adhesive polarization in collision processes, as shown in Fig. 1(b). The directed protrusion then synchronizes the movement of gathered cells, and is ultimately expected to bring about collective migration.

To test this expectation, the potential of polarized cell-cell adhesion as a communication tool in collective cell migration is theoretically explored. Indeed, such polarization does appear to result in the gathering of model cells while further providing them with collective propulsion with persistence, even when a cell in isolation only exhibits random-walk movement without persistence. Through this propulsion, the model cells switch their motion from random to collective with a sufficient strength of polarized cell-cell adhesion.

Let us first consider the case of cells with the unit vector of polarity direction \mathbf{p} in cell-cell adhesion. To properly lead other cells, a cell should adjust \mathbf{p} using the information of movement. A hypothesis for this adjustment mechanism is that \mathbf{p} simply follows the protrusion or the inducing motion of a cell, as shown in Fig. 1(c). This is formulated by

$$\frac{d\mathbf{p}}{dt} = -\eta\mathbf{p} \times \left(\mathbf{p} \times \frac{d\mathbf{R}}{dt} \right) \quad (1)$$

Here, t is time and \mathbf{R} is the position of the cell. This equation induces a high correlation between \mathbf{p} and $d\mathbf{R}/dt$ through a positive feedback loop (Fig. 1(d)). This hypothetical feedback has been observed during the early development of *Dictyostelium discoideum* [31]. Eq. (1) is employed as a working conjecture for mechanism exploration.

To facilitate the theoretical exploration, an artificial model of cultured cells on a two-dimensional (2D) medium is considered, according to the 2D cellular Potts model [32, 33]. This model generates a probable amoeba cell configuration by a Monte Carlo method and enables the sampling of probable cell configurations. In this model, the cell configurations are represented by Potts states $m(\mathbf{r})$, representing the state at a site \mathbf{r} on a square lattice with a linear dimension of L . The set of all $m(\mathbf{r})$ values is denoted by $\{m(\mathbf{r})\}$. $m(\mathbf{r})$ takes on a number in $\{0, 1, \dots, N\}$. When $m(\mathbf{r}) = 0$, \mathbf{r} is empty; otherwise, \mathbf{r} is occupied by the $m(\mathbf{r})$ th cell. Hence, the domain of $m(\mathbf{r}) = m$ determines the shape of the m th cell. N is the number of cells. For simplicity in the present exploration, a constant N is assumed by ignoring the effects of cell division and death.

Using this model, the possible configurations of cells are sampled based on Monte Carlo simulation with a probability of realization for $\{m(\mathbf{r})\}$. The probability $P(\{m(\mathbf{r})\})$ is proportional to $\exp(-\beta\mathcal{H}(\{m(\mathbf{r})\}))$. Here, β is a parameter of cell motility and $\mathcal{H}(\{m(\mathbf{r})\})$ is energy defined by

$$\begin{aligned} \mathcal{H}(\{m(\mathbf{r})\}) = & \sum_{\langle \mathbf{r}, \mathbf{r}' \rangle} J_{\mathbf{r}\mathbf{r}'} [1 - \delta_{m(\mathbf{r})m(\mathbf{r}')}] \\ & + \kappa \sum_{m=1}^{N_{\text{Cell}}} (V_m - V)^2. \end{aligned} \quad (2)$$

The first term on the right-hand side represents energies derived from the tension of the cell periphery in the medium and the tension of cell-cell contact [34, 35]. In this term, the summation of $\langle \mathbf{r}, \mathbf{r}' \rangle$ is taken over all neighboring site pairs, consisting of the nearest and next-nearest neighbor site pairs [32]. $\delta_{mm'}$ is the Kronecker delta. $J_{\mathbf{r}\mathbf{r}'}$ is the strength of the interface tension between \mathbf{r} and \mathbf{r}' . The second term on the right-hand side represents the area stiffness energy. By this term, the area of the m th cell, $V_m = \sum_{\mathbf{r}} \delta_{m(\mathbf{r})m}$, is maintained to be a certain value, V . Here, κ is the stiffness of the area.

This cellular Potts model has been used for expressing various polarized cell-cell adhesion events [36–38]. To

express the single-side polarized cell-cell adhesion shown in Fig. 1(a), as $J_{\mathbf{r}\mathbf{r}'}$ in Eq. (2), Eq. (12) from Ref. [38] is adopted:

$$J_{\mathbf{r}\mathbf{r}'} = J_{m(\mathbf{r})m(\mathbf{r}')} - J_p w_m(\mathbf{r}) w_{m'}(\mathbf{r}'), \quad (3)$$

where $w_m(\mathbf{r}) = (1 + \mathbf{p}_m \cdot \mathbf{e}_m(\mathbf{r})) \eta_{m0}/2$, $J_{mm'} = J_{\text{CM}} [\delta_{m0}\eta_{m'0} + \eta_{m0}\delta_{m'0}] + J_{\text{CC}} \eta_{m0} \eta_{m'0}$, and $\eta_{ab} = 1 - \delta_{ab}$. J_{CM} is the tension of the cell periphery, J_{CC} is the strength of isotropic cell-cell adhesion, and J_p is the strength of polarized cell-cell adhesion. \mathbf{p}_m is a unit vector representing polarization of the m th cell in cell-cell adhesion. $\mathbf{e}_m(\mathbf{r})$ is a unit vector from the center of the m th cell, \mathbf{R}_m , to a position on the cell periphery, \mathbf{r} . Concretely, it is defined by $(\mathbf{r} - \mathbf{R}_m) / |\mathbf{r} - \mathbf{R}_m|$. Here, $\mathbf{R}_m = \sum_{\mathbf{r} \in \Omega_m} \mathbf{r} / V_m$, where Ω_m is the set of all the sites occupied by the m th cell. In Eq. (3), \mathbf{p}_m obeys the 2D version of Eq. (1):

$$\frac{d\mathbf{p}_m}{dt} = \eta \left[\frac{d\mathbf{R}_m}{dt} - \left(\frac{d\mathbf{R}_m}{dt} \cdot \mathbf{p}_m \right) \mathbf{p}_m \right]. \quad (4)$$

With this model, the time series of cell configuration is generated by the following conventional Monte Carlo process. In this process, a Monte Carlo step is iterated and produces amoeba cell motion. The single Monte Carlo step consists of $16 \times L^2$ copies of a state from a source site \mathbf{r}' to a trial site \mathbf{r} . For each copy, this trial site \mathbf{r} is randomly chosen among all sites. Then, a source site, \mathbf{r}' , is selected randomly among neighboring sites of \mathbf{r} . The state copy of $m(\mathbf{r}')$ from \mathbf{r}' to \mathbf{r} is accepted with the Metropolis probability of

$$\begin{aligned} & P(\{m_c(\mathbf{r})\} | \{m(\mathbf{r})\}) \\ & = \min [1, P(\{m_c(\mathbf{r})\}) / P(\{m(\mathbf{r})\})]. \end{aligned} \quad (5)$$

Otherwise, it is rejected. Here, $\{m_c(\mathbf{r})\}$ is the state in which the state is copied from \mathbf{r}' to \mathbf{r} .

For the integration of Eq. (4), the Euler method is employed. In addition, the adiabatic approximation is employed, where the equation is integrated only between two consecutive Monte Carlo steps. This approximation is based on the assumption that the change of \mathbf{p}_m is much slower than the rate of a single flip. To maintain consistency between time scales in Eq. (4), it is assumed that \mathbf{R}_m is an adiabatic value and is a constant during each Monte Carlo step. \mathbf{R}_m is also calculated with each integration of Eq. (4).

Note that this model does not include the propulsion term of individual cells. Namely, these model cells only exhibit random-walk movement without persistence when in isolation. Nevertheless, at high density, these cells may collectively acquire propulsion with persistence if the polarized cell-cell adhesion functions as a leading communication tool.

Even if cells acquire the collective propulsion with persistence, it is only expected for a limited set of model parameters. In particular, the area fraction of cells $\phi = NV/L^2$ is a control factor because a small ϕ reduces the cell-cell adhesion effects. Therefore, the appropriate

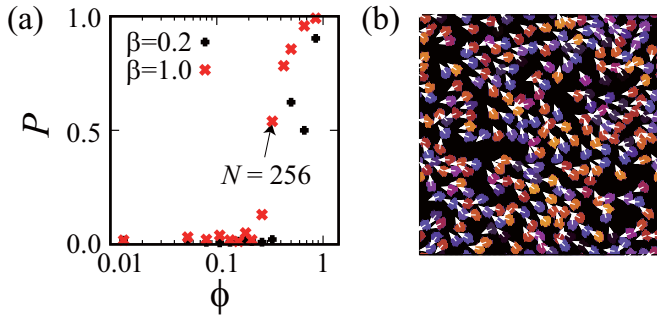


FIG. 2. (a) Order parameter of polarity P as a function of the area fraction ϕ . (b) Snapshot of $\{m(\mathbf{r})\}$ and \mathbf{p}_m s at $N = 256$ ($\phi = 42\%$) and $\beta = 0.5$. The colored region indicates cells. Different colors represent different cells. The black region represents empty space. White arrows represent the direction of polarized cell-cell adhesion.

value of ϕ is first determined for the present exploration. As a possible probe of this propulsion, the average value of \mathbf{p}_m is considered,

$$P = \frac{1}{TN} \left| \sum_m \sum_{t=t_0}^{t_0+T} \mathbf{p}_m(t) \right|. \quad (6)$$

Since \mathbf{p}_m reflects cell motion through Eq. (4), P is expected to reflect the emergence of collective propulsion. Here, t_0 is a starting time of the time average of \mathbf{p}_m . To access a steady state, we can set $t_0 = 5 \times 10^5$ steps, and simulate the relaxation from cells forming a single aggregation with a random configuration of \mathbf{p}_m s up to the time. We can also set $T = 2 \times 10^5$ to calculate the mean square displacement, D^2 , over the long term, as described below. Here, the proper value of ϕ is explored by calculating the ϕ -dependence of P in the corresponding range of N from 1 to 512 with $V = 64$ and $L = 196$. In this case, the periodic boundary condition is adopted, which enables cells to freely move through the boundary.

In this simulation, the adhesion parameters are set to $J_{CM} = 2.0$, $J_{CC} = 5.0$, and $J_p = 2.0$ to represent the cell model shown in Fig. 1(a). With these parameters, cells extend their interface during contact between their front sides and contract their interface during contact of their rear sides. Here, the front side of a cell is defined according to the peripheral edge of the cell in the direction of polarized cell-cell adhesion; the rear side is that opposite to the front side. For numerical stability, $\eta = 0.1$, and $\kappa = 1$ and $\beta = 0.2$ or $\beta = 0.5$ are chosen.

P is plotted as a function of ϕ in Fig. 2(a). For small ϕ , P takes on a small value. As ϕ increases up to around 0.3, P rapidly increases. With further increases in ϕ , P gradually reaches unity, indicating the progression of \mathbf{p}_m ordering. This transition of P reflects the collective motion occurring for large ϕ and its underlying propulsion. To gain insight into \mathbf{p}_m s, a snapshot of $\{m(\mathbf{r})\}$ and \mathbf{p}_m s is shown in a relaxed state for $N = 256$ ($\phi = 42\%$) in

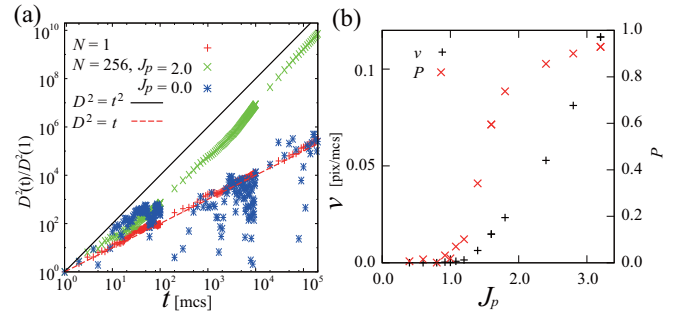


FIG. 3. (a) D^2 as a function of the time step t . D^2 is scaled by D^2 at the time step $t = 1$ for data sorting. The symbol $+$ represents the D^2 for isolated cells, which is averaged over 64 cells. The symbol \times represents the D^2 for $J_p = 2.0$. The symbol $*$ represents the D^2 for $J_p = 0.0$. (b) v and P as a function of J_p .

Fig. 2(b). The polarities of \mathbf{p}_m s are indicated by arrows that exhibit ordering.

Next, to address the propulsion of this collective motion and its persistence, the D^2 is calculated and averaged across the cells.

$$D^2 = \frac{1}{N} \sum_m |\mathbf{R}_m(t_0 + t) - \mathbf{R}_m(t_0)|^2 \quad (7)$$

When cells have propulsion with persistence, they exhibit ballistic motion during a short period; therefore, D^2 behaves as $D^2 \sim t^2$. Otherwise, the cells diffusively move, and therefore D^2 behaves as $D^2 \sim t$. Here, we will concentrate on the case of $\beta = 0.5$ to clearly observe the stable motion in comparison with the case of low β .

D^2 is shown as a function of t in Fig. 3(a). D^2 for cells with polarized adhesion ($J_p = 2.0$) behaves as $D^2 \sim t^2$. In contrast, D^2 for isolated cells and that for cells with isotropic adhesion ($J_p = 0.0$) behave as $D^2 \sim t$. These contrasting results suggest that the model cells collectively acquire propulsion with persistence by using polarized cell-cell adhesion.

The time period of $D^2 \sim t^2$ in Fig. 3(a) is unexpectedly long. This implies a stable order in collective motion. To directly confirm this ordering due to polarized cell-cell adhesion, the average velocity is calculated as

$$v = \frac{1}{NT} \left| \sum_{m,t} \frac{d\mathbf{R}_m(t)}{dt} \right|, \quad (8)$$

and is plotted as a function of J_p in Fig. 3(b) with P . v at $J_p = 0$ is equal to 0. As J_p increases up to 1, v is almost 0. As J_p further increases beyond $J_p = 1$, v gradually increases along with J_p and P . These observations indicate that a stable order in collective motion occurs for $J_p > 1$. Overall, these results imply that polarized cell-cell adhesion enables the model cells to switch their motion from random to collective at a threshold of J_p .

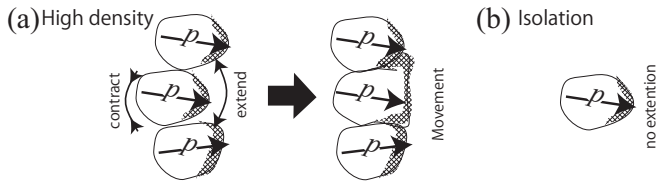


FIG. 4. Schematic diagram of collective propulsion in the cases of (a) high cell density and (b) an isolated cell. The arrows of \mathbf{p} represent the direction of polarized cell-cell adhesion, and the shaded region represents the high-strength region of cell-cell adhesion.

In conclusion, these results provide a theoretical demonstration that polarized cell-cell adhesion can function as the source of collective propulsion with persistence. This suggests that cells can mutually lead themselves into a state of collective cell migration using polarized cell-cell adhesion.

The emergence of collective propulsion is a notable physical phenomenon, but its mechanism of origin is still largely a mystery. A key to solving this mystery is consideration of the role played by the tension gradient inducing propulsion [39]. To intuitively approach this question, let us consider the periphery tension of a cell (here, we will choose the m th cell) that is completely surrounded by other cells. For such a cell, the tension term proportional to $\sum_{\mathbf{r}} \mathbf{p}_m \cdot \mathbf{e}_m(\mathbf{r})$ in Eq. (3) indicates that the tension on the front side is smaller than that on the rear side of the cell. Therefore, a cell extends or protrudes from its front side as shown in Fig. 4(a). In contrast, a cell comparatively contracts on the rear side. These extensions and contractions induce the propulsion of a cell in the

direction of \mathbf{p}_m . This phenomenon is the origin of the emergent propulsion. In contrast to this case, since a cell in isolation only experiences isotropic tension, as shown in Fig. 4(b), it exhibits a simple random walk.

Since this mechanism only accounts for the emergence of collective propulsion at high density, it is insufficient to explain the ordering of movement shown in Fig. 3(b). The positive feedback control in Fig. 1(d) plays a significant role as the origin of the persistence of propulsion to induce this ordering. This can be reasoned as follows. The polarity of adhesion \mathbf{p} effectively acts as the cell polarity of movement [16] by inducing energy that is proportional to $\sum_{\mathbf{r}} \mathbf{p}_m \cdot \mathbf{e}_m(\mathbf{r})$, as discussed above. Further, the positive feedback control in Eq. (1) induces the persistence of cell polarity [40], which is well known to induce the ordering of movement [41], to ultimately result in the observed ordering.

This emergent collective propulsion may have an essential function in driving collective motion. As described above, cells can theoretically switch their motion from random to ordering by utilizing cell-cell adhesion. Indeed, polarization in cell-cell adhesion has been shown to arise in the aggregating process of *Dictyostelium discoideum* [42], which might have functioned as a trigger of collective motion in evolutionary history. Since confirmation of the function of polarization throughout evolutionary history is difficult, further theoretical exploration of these relationships controlling for the effects of chemotaxis would be an important topic of future research.

This work is supported by JSPS KAKENHI Grant Number 15K17740. The author would like to thank Ryosuke Ishiwata, Hidekazu Kuwayama, Daisuke Mashiko, Shunsuke Yabunaka, and Kenichi Hironaka for meaningful discussions. The author also thanks Koichi Fujimoto, Macoto Kikuchi, and Hajime Yoshino for their generous support.

-
- [1] C. J. Weijer, *J. Cell Sci.* **122**, 3215 (2015).
 [2] P. Friedl and D. Gilmour, *Nat. Rev. Mol. Cell Biol.* **10**, 445 (2009).
 [3] P. Rørth, *Annu. Rev. Cell Dev. Biol.* **25**, 407 (2009).
 [4] A. Haeger, K. Wolf, M. M. Zegers, and P. Friedl, *Trends Cell Biol.* **25**, 556 (2015).
 [5] J. A. Sherratt and J. D. Murray, *Proc. R. Soc. London, Ser. B* **241**, 29 (1990).
 [6] B. Szabó, G. J. Szollosi, B. Gonci, Z. Juranyi, D. Selmecezi, and T. Vicsek, *Phys. Rev. E* **74**, 061908 (2006).
 [7] P. Lee and C. W. Wolgemuth, *PloS Comput. Biol.* **7**, e1002007 (2011).
 [8] P. Lee and C. Wolgemuth, *Phys. Rev. E* **83**, 061920 (2011).
 [9] T. Vicsek and A. Zafeiris, *Phys. Rep.* **517**, 71 (2012).
 [10] M. Basan, J. Elgeti, E. Hannezo, W.-J. Rappel, and H. Levine, *Proc. Natl. Acad. Sci. USA* **110**, 2452 (2013).
 [11] M. C. Marchetti, J. F. Joanny, S. Ramaswamy, T. B. Liverpool, J. Prost, M. Rao, and R. A. Simha, *Rev. Mod. Phys.* **85**, 1143 (2013).
 [12] N. Sepúlveda, L. Petitjean, O. Cochet, E. Grasland-Mongrain, P. Silberzan, and V. Hakim, *PloS Comp. Biol.* **9**, e1002944 (2013).
 [13] B. Li and S. X. Sun, *Biophys. J.* **107**, 1532 (2014).
 [14] C. Londono, M. J. Loureiro, B. Slater, P. B. Lückner, J. Soleasa, S. Sathananthan, J. S. Aitchison, A. J. Kabla, and A. P. McGuigan, *Proc. Natl. Acad. Sci. USA* **111**, 1807 (2014).
 [15] B. A. Camley, J. Zimmermann, H. Levine, and W.-J. Rappel, *Phys. Rev. Lett.* **116**, 098101 (2016).
 [16] A. J. Kabla, *J. R. Soc. Interface* **9**, 3268 (2012).
 [17] C.-M. Lo, H.-B. Wang, M. Dembo, and Y. li Wang, *Biophys. J.* **79**, 144 (2000).
 [18] S. B. Carter, *Nature* **5073**, 256 (1967).
 [19] E. Méhes and T. Vicsek, *Comput. Adapt. Syst. Mod.* **1**, 4 (2013).
 [20] W. Pfeffer, *Umtersuch. Bot. Inst. Tübingen.* **1**, 363 (1884).
 [21] J. T. Bonner, *The Social Amoebae: The Biology of Cellu-*

- lar Slime Molds* (Princeton University Press, Princeton, 2009).
- [22] C. Carmona-Fontaine, H. K. Matthews, S. Kuriyama, M. Moreno, G. A. Dunn, M. Parsons, C. D. Stern, and R. Mayor, *Nature (London)* **456**, 957 (2008).
- [23] K. F. Swaney, C.-H. Huang, and P. N. Devreotes, *Annu. Rev. Biophys.* **39**, 265 (2010).
- [24] M. Takeichi, *Nat. Rev. Mol. Cell. Biol.* **15**, 397 (2014).
- [25] J. G. Dumortier, S. Martin, D. Meyer, F. M. Rosa, and N. B. David, *ProcProc* **109**, 16945 (2012).
- [26] D. Cai, S.-C. Chen, M. Prasad, L. He, X. Wang, V. Choismel-Cadamuro, J. K. Sawyer, G. Danuser, and D. J. Montell, *Cell* **157**, 1146 (2014).
- [27] P. Friedl and K. Wolf, *Nat. Rev. Cancer* **3**, 362 (2003).
- [28] H. Beug, F. E. Katz, and G. Gerisch, *J. Cell Biol.* **56**, 647 (1973).
- [29] K. Müller and G. Gerisch, *Nature (London)* **274**, 445 (1978).
- [30] E. Theveneau, *Dev. Cell.* **19**, 39 (2010).
- [31] H. Sesaki and C.-H. Siu, *Develop. Biol.* **177**, 504 (1996).
- [32] F. Graner and J. A. Glazier, *Phys. Rev. Lett.* **69**, 2013 (1992).
- [33] A. R. A. Anderson, M. A. J. Chaplain, and K. A. Rejniak, *Single-Cell-Based Models in Biology and Medicine* (Birkhauser Verlag AG, Basel, 2007).
- [34] J. A. Glazier and F. Graner, *Phys. Rev. E* **47**, 2128 (1993).
- [35] F. Graner, *J. Theor. Biol.* **164**, 455 (1993).
- [36] M. Zajac, G. L. Jonesa, and J. A. Glazier, *J. Theor. Biol.* **222**, 247 (2002).
- [37] R. M. A. Vroomans, P. Hogeweg, and K. H. W. J. ten Tusscher, *PLoS Comput. Biol.* **11**, e1004092 (2015).
- [38] K. Matsushita, *Phys. Rev. E.* **95**, 032415 (2017).
- [39] M. D. Levan, *J. Coll. Int. Sci.* **83**, 11 (1981).
- [40] A. Czirók, K. Varga, E. Méhes, and A. Szabó, *New J* **15**, 075006 (2013).
- [41] J. Deseigne, O. Dauchot, and H. Chaté, *Phys. Rev. Lett.* **105**, 098001 (2010).
- [42] J. C. Coates and A. J. Harwood, *J. Cell Sci.* **114**, 4349 (2001).